Progress In Electromagnetics Research, Vol. 148, 233–243, 2014

Multiband Frequency Reconfigurable 4G Handset Antenna with MIMO Capability

Janne Ilvonen[1, *], Risto Valkonen[2], Jari Holopainen[1], and Ville Viikari[1]

Abstract—A novel frequency reconfigurable 4G Multiple-Input Multiple-Output (MIMO) handset antenna is presented and verified with experimental results. Frequency tuning is used to minimize the antenna volume and to compensate for the losses related to user-originated impedance detuning. Both antenna elements are independently frequency reconfigurable and can cover most of the LTE-A bands. The study compares the losses of CMOS- and MEMS-based digitally tunable capacitors (DTC). In addition, two prototypes with total antenna volumes of 1170 and 3900 mm^3 have been studied. The results show that the larger antenna structure operates with an efficiency better than 49% across the frequencies of 698–960 MHz and better than 56% across the frequencies of 1430–2690 MHz, when a MEMS-based DTC is used. In addition, a new method is introduced to estimate the suitability of the antenna geometry for frequency tunable antennas.

1. INTRODUCTION

The number of antennas in small mobile devices has been continuously increasing along with the frequency band allocated for cellular use, while the volume reserved for the antennas has remained the same or even reduced. As a consequence, antennas easily become inefficient, thereby significantly lowering the achievable data rates and coverage. One possible solution to this challenge is to use small, frequency reconfigurable antennas to instantaneously cover only a part of the used band(s). The feasibility of this approach has significantly increased due to the recent developments in Complementary Metal Oxide Semiconductor (CMOS) and MicroElectroMechanical Systems (MEMS) technologies.

Several handset antennas with multi-antenna functionality have been proposed in recent years, such as the MIMO antennas presented in [1–6]. In addition, a number of frequency reconfigurable handset antennas have been proposed, e.g., in [5, 7–10]. Based on the authors' knowledge, there are only a few previous papers with measurement results dealing with a frequency reconfigurable handset antenna having MIMO performance [5, 10].

In [5], frequency tuning is achieved by using a planar inverted-F antenna (PIFA) with a four-state GaAs switch. The structure is large in size (8750 mm^3) and only the main antenna is frequency reconfigurable. In [10], frequency tuning is implemented by using a PIFA with a varactor diode. However, the tuning range is limited and the antenna efficiency is not reported.

In this paper, a novel frequency reconfigurable handset antenna with MIMO capability is presented. Two prototypes with total antenna volumes of 1170 and 3900 mm^3 are studied. In addition, a new way of analyzing the suitability of the antenna geometry for frequency tuning is introduced. The matching circuit losses of CMOS- and MEMS-based DTCs are discussed.

Preliminary antenna structures studied are shown in Section 2. The used matching circuit and the losses caused by the tuning are presented in Section 3. It is shown that a close correlation exists between the reactance behavior of the antenna input impedance and the tuning circuit losses. The final

Received 27 June 2014, Accepted 5 August 2014, Scheduled 20 August 2014

* Corresponding author: Janne Ilvonen (janne.ilvonen@aalto.fi).

[1] Department of Radio Science and Engineering, School of Electrical Engineering, Aalto University, Espoo, AALTO FI-00076, Finland.

[2] University of Kiel, Institute of Electrical and Information Engineering, Chair of Wireless Communications, Kiel, Germany.

antenna structure and the manufactured prototypes are presented and discussed in Section 4, in which different performance metrics with and without the presence of a user are shown and explained. Finally, the proposed design is compared to state-of-the-art antennas.

2. ANTENNA DESIGN

2.1. Envelope Correlation and Multiplexing Efficiency

The envelope correlation coefficient (ρ_e) defines the similarity between antenna patterns, and it is often required that $\rho_e < 0.5$ in order to provide good diversity and spatial multiplexing efficiency. In the analysis of this work, the ρ_e is calculated from radiation patterns using the equation presented in [11] assuming isotropic and uniform, i.e., reflection-rich environment. The complex far-field radiation patterns are measured in an anechoic chamber. It is shown in [12] that the spatial multiplexing efficiency ($\tilde{\eta}_{mux}$) in an isotropic environment is

$$\tilde{\eta}_{mux} = \sqrt{\eta_1 \eta_2 (1 - \rho_e)} \tag{1}$$

where η_1 and η_2 are the total efficiencies of the antenna elements 1 and 2, respectively. The $\tilde{\eta}_{mux}$ defines the loss of signal-to-noise ratio (SNR) with respect to ideal MIMO antennas. The approximation is made under an assumption that the SNR is greater than 15–20 dB. When the SNR is lower, diversity techniques are typically applied.

2.2. Design Considerations

The antennas are designed with the LTE-A specifications in mind. The LTE-A band is divided into two sub-bands: (1) 698–960 MHz (later "low-band") and (2) 1430–2690 MHz (later "high-band"). The bandwidth requirement at the low-band is 262 MHz, and in order to achieve this demand, a relatively large antenna volume is required [6]. In this paper, frequency tuning is used to minimize the required antenna volume and to compensate for the losses related to user-originated impedance detuning. The use of non-self-resonant elements [13] is justified due to their low inherent selectivity, which makes their frequency tunability more prominent compared to self-resonant elements [7, 8]. Furthermore, non-resonant antennas require the use of matching circuits in any case, meaning that tunability will not add much to the complexity of matching circuit. The tuning will be implemented by using two different types of DTCs [14, 15].

The antenna geometry is printed on a $120 \times 60 \times 1.5\,\text{mm}^3$ PCB ground plane (Rogers RO4003C) with copper coating on both sides. The area reserved for each antenna is $15 \times 26(390)\,\text{mm}^2$, and space for a USB port is reserved between the antennas. The studied antenna structures are placed inside a polycarbonate enclosure with total outer dimensions of $122 \times 62 \times 7\,\text{mm}^3$. The PCB is located close to the back cover, as shown in Figure 5(c). All electromagnetic (EM) simulations in this paper are performed using the FDTD-based EM-simulator SEMCAD-X by SPEAG.

In conventional Single-Input Single-Output (SISO) antenna systems, the main parameters affecting the antenna performance at the low-band are the size of the antenna element and chassis [6, 16]. In addition, the location of the antenna element has a significant contribution to the antenna performance. The location of the feedings also has a major effect on the MIMO performance [3]. The shape of the antenna element affects the impedance behavior which has strongly influences the tuning range and component losses, as will be shown later.

A major challenge in electrically small, frequency reconfigurable antennas is often to achieve a reasonable efficiency at low frequencies while maintaining an adequate tuning range. Therefore, the focus in this paper is to have as good a total efficiency as possible at low bands, while having a sufficient frequency tuning range to cover most of the LTE-A bands.

2.3. Antenna Feed, Shape, and Dimensions

Next, we demonstrate using three generic antenna structures ($\mathcal{A}$, $\mathcal{B}$ and $\mathcal{C}$) how to end up with the final antenna design (see Figure 1). The antenna geometries are designed to have a strong coupling to the lowest-order chassis wavemodes and to maximally utilize the available antenna volume. Two extreme

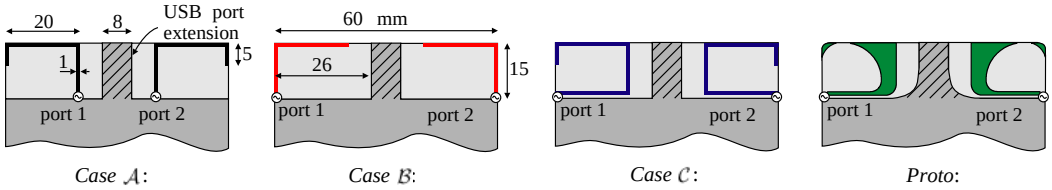

Figure 1. Studied antenna cases. *Cases* $\mathcal{A}$–$\mathcal{C}$ are planar, whereas *Proto* has a height of 5 mm.

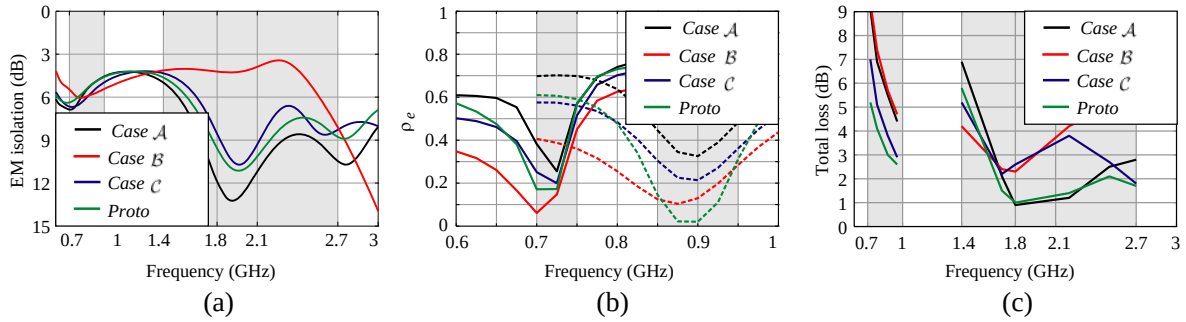

Figure 2. Simulated (a) EM isolation, (b) ρ_e, and (c) total loss with the CMOS-based DTC.

feeding locations have been studied. Three different performance metrics for the antennas are shown in Figure 2: 1) electromagnetic (EM) isolation; 2) ρ_e; and 3) total loss (L_{tot}).

1) **EM Isolation** defines the isolation between antenna elements in a theoretical case where all elements are perfectly matched with lossless matching circuits [17]. The USB extension (Figure 1) improves the EM isolation by 2–3 dB at the low-band compared to the case without the extension. As shown in Figure 2(a), the location of the feed does not have a significant effect on the EM isolation (*Cases* $\mathcal{A}$ and $\mathcal{C}$), whereas the antenna geometry has a strong influence on the EM isolation performance — the open ends of the antenna should be pointing away from each other, as with *Cases* $\mathcal{A}$ and $\mathcal{C}$.

2) **Envelope correlation** is determined when the antenna elements are in resonance ($|S_{11}| \approx -18$ dB) at 0.7 and 0.9 GHz. The matching is realized with a lossless L-section matching circuit at 720 and 900 MHz. As seen in Figure 2(b), the best ρ_e performance is achieved when the antenna feeds are placed far from each other (*Cases* $\mathcal{B}$ and $\mathcal{C}$). This is due to the diagonal antenna-chassis mode introduced in [18].

3) **Total loss** results shown in Figure 2(c) are calculated by using the optimal DTC value in each studied frequency point, i.e., the antenna is matched separately at each frequency point with Optenni Lab circuit simulator [19]. The used matching circuit topology is shown in Figure 3, and a CMOS-based DTC is used. At 700–800 MHz, the losses are mainly caused by the matching circuit. At 800–1000 MHz, the isolation losses are about the same order of magnitude as the component losses. At the high band, the mismatch losses are significant in most cases, i.e., the tuning range is not sufficient (*Cases* $\mathcal{B}$ and $\mathcal{C}$). The location of the feeds does not affect the total loss (L_{tot}) performance, whereas the antenna geometry has the most significant impact on the L_{tot} behavior. The reason for this is studied further in the next section.

3. ANTENNA GEOMETRY

The used antenna element is inherently capacitive across most of the LTE-A bands that it should cover. One possible dual-band matching circuit topology that can cover the desired bands is presented in [20]. This matching circuit combines the performance of low-pass and high-pass resonators (see Figure 3). The frequency tuning is realized by varying the state of the shunt capacitor, which is later denoted as a digitally tunable capacitor (DTC).

For efficient performance of the tuning circuit, the antenna impedance should be chosen properly. A traditional way is to use the antenna Q to estimate the efficiency of the antenna structure [21].

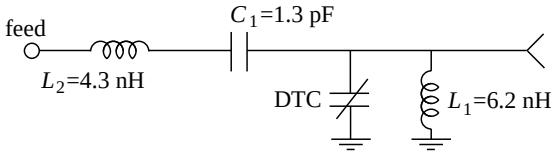

Figure 3. Circuit schematic for the tunable antenna and the component values used.

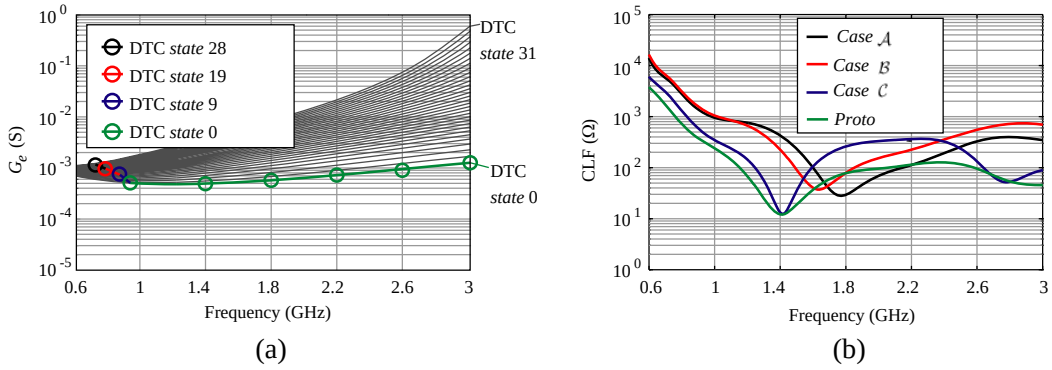

Figure 4. (a) Ratio of the effective conductance, (b) CLF of the studied antennas.

Typically, a large antenna Q results in high resistive losses of the antenna structure and matching circuit. However, this method does not necessarily lead to the best antenna geometry for frequency reconfigurable antennas. The Q of *Cases* $\mathcal{A}$, $\mathcal{B}$ and $\mathcal{C}$ is 23.8, 24.0, and 26.0, respectively, at 720 MHz. Although *Case* $\mathcal{C}$ has the highest Q of the three at the example frequency, it performs best in terms of L_{tot} when the tuning circuit is employed (see Figure 2(c)).

Numerical study on the losses of the matching circuit revealed that the DTC and inductor L_1 dominate the total resistive losses at all frequencies and DTC states. Hence, the total resistive losses, when possible impedance mismatch losses are not included, can be approximated as

$$L_{\text{P}} = 1 + G_{\text{e}}/G_{\text{L}} = 1 + \frac{R_{\text{e}}}{R_{\text{e}}^2 + X_{\text{e}}^2}\frac{R_{\text{L}}^2 + X_{\text{L}}^2}{R_{\text{L}}} \tag{2}$$

where G_{e} is the total conductance of the DTC and L_1, and G_{L} is the radiation conductance of the antenna. Figure 4(a) shows $G_{\text{e}} = R_{\text{e}}/(R_{\text{e}}^2 + X_{\text{e}}^2)$ for CMOS-based DTC. Note that G_{e} is a function of frequency and state of the DTC. The capacitance of the DTC increases with the state such that state 31 is used at the lowest frequency and state 0 at the highest one. In the low-band, G_{e} is between 10^{-3} and $5 \cdot 10^{-4}$, varying relatively little across the whole frequency band, and thus its effect can be neglected. Finally, the efficiency of the matching circuit is inversely proportional to the radiation conductance of the antenna. The Conductance Loss Factor (CLF) for the most promising antenna geometry can be derived from (2) and can be expressed as

$$\text{CLF} = \frac{1}{G_{\text{L}}} = \frac{R_{\text{L}}^2 + X_{\text{L}}^2}{R_{\text{L}}}. \tag{3}$$

In general, a better tuning circuit efficiency is obtained with a lower CLF. The CLF corresponds well with the L_{tot} results shown in Figure 2(c), especially at the low-band. At the high-band, the comparison is not as straightforward because of the matching losses that are included in the L_{tot}.The resistive losses were ignored in the simulations ($R_{\text{rad}} = R_{\text{L}}$).

4. PROTOTYPE DESIGN

The preliminary study with *Cases* $\mathcal{A}$, $\mathcal{B}$ and $\mathcal{C}$ revealed that the feeding points should be placed far from each other to improve the ρ_e. In addition, the open ends should be located far from each other

to improve the EM isolation. The loss study revealed that the best η_{tot} is achieved when the radiation conductance of the antenna element remains at a reasonable level across the whole band. Thus, *Case* $\mathcal{C}$ is the best candidate to be studied further. However, the performance of *Case* $\mathcal{C}$ near 2.2 GHz is limited (see Figure 2(c)). This is mainly due to a large series inductance caused by the long and thin feeding strip (length 35 mm). This can be avoided by using a curved feed that decreases the effective series inductance and keeps the effective parallel capacitance suitable. One possible way to reduce feed inductance through shape optimization is shown in Figure 1 (*Proto*).

The used fixed-value matching components are from the LQW18A and GQM1885 series by Murata. Two different DTC types are studied: the first is the CMOS-based PE64904 by Peregrine [14] and the second is the MEMS-based WS1050 by WiSpry [15]. The quality factors of the DTCs are from 10 to 35 (CMOS) and from 120 to 590 (MEMS), and the capacitance tuning range is from 1.14 to 5.10 pF and 0.50 to 5.75 pF, respectively.

Based on the above discussion, a prototype was designed, fabricated and measured (see Figure 5). The antenna elements are located symmetrically with respect to the long axis of the chassis in order to simplify the implementation of the matching circuit. Hence, the elements are located on opposite sides of the PCB. Each individual antenna design is referred to with a letter, e.g., "*ProtoC*", where *C* refers to CMOS-based DTC and *M* to MEMS-based DTC used in the design. The measurements were made only for *ProtoC* because of limited availability of the MEMS-based DTC at that time.

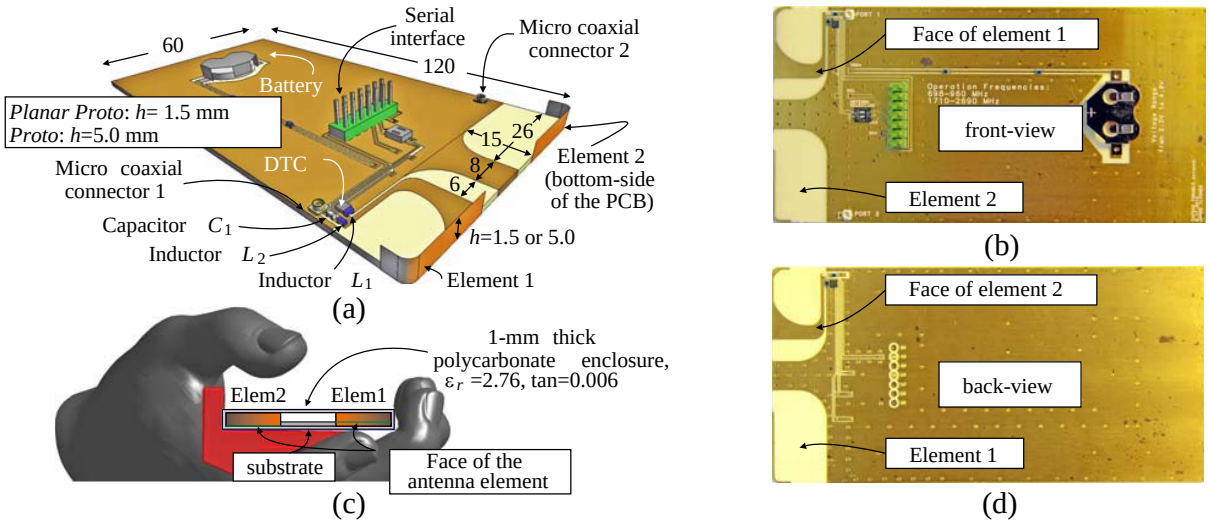

Figure 5. (a) Schematic view of the antenna structure. (b) Front-view of the fabricated prototype (*ProtoC*). (c) Antenna placed inside a polycarbonate enclosure and its position respect to the enclosure and phantom hand. (d) Back-view of the fabricated prototype (*ProtoC*). Dimensions are in mm.

4.1. Matching Circuit Losses

The distribution of the matching circuit losses is further analyzed in Table 1 which compares the two DTCs at different frequencies. The isolation efficiency (η_{isol}) includes the coupling losses between the antennas and the component losses of port 2. The matching (η_{m}) and series component efficiencies are negligible. The efficiencies are determined using Optenni Lab. As can be seen in Table 1, a significant portion of the losses is caused by the shunt inductor (L_1) in addition to those of the DTC. The purpose of L_1 is to tune the antenna to the correct frequency band, meaning that a relatively large current flows through the component (especially at the low-band). Nevertheless, the components have to be placed this way to establish the desired tuning range. The losses of CMOS-based DTC are very high (2.9 dB) at the low-band, as already suggested by its low Q. On the other hand, the losses of MEMS-based DTC are significantly smaller (less than 0.5 dB).

Table 1. Loss study of *Proto*. The efficiencies are calculated when element 1 is transmitting and element 2 is connected to a 50-Ω termination. The elements are working at the same frequency.

DTC model	freq (MHz)	Simulated η_{DTC} (dB)	Simulated η_{L_1} (dB)	Simulated η_{isol} (dB)	Simulated η_{tot} (dB)	Measured η_{tot} (dB)
CMOS [14]	720	−2.9	−2.1	−0.2	−5.2	−5.2
	770	−1.9	−1.6	−0.5	−4.1	−4.2
	850	−0.9	−1.0	−0.9	−3.0	−3.7
	920	−0.4	−0.7	−1.4	−2.6	−3.0
	1700	−0.1	−0.0	−0.6	−1.3	−1.9
	2000	−0.2	−0.1	−0.3	−1.0	−1.3
	2500	−0.5	−0.1	−0.4	−2.3	−2.4

DTC model	freq (MHz)	Simulated η_{DTC} (dB)	Simulated η_{L_1} (dB)	Simulated η_{isol} (dB)	Simulated η_{tot} (dB)	Measured η_{tot} (dB)
MEMS [15]	720	−0.5	−1.8	−0.1	−2.4	N/A
	770	−0.3	−1.0	−0.4	−1.8	N/A
	850	−0.1	−0.6	−0.8	−1.4	N/A
	920	−0.0	−0.4	−1.2	−1.8	N/A
	1700	−0.1	−0.1	−0.3	−1.4	N/A
	2000	−0.1	−0.1	−0.3	−0.7	N/A
	2500	−0.1	−0.1	−0.4	−1.5	N/A

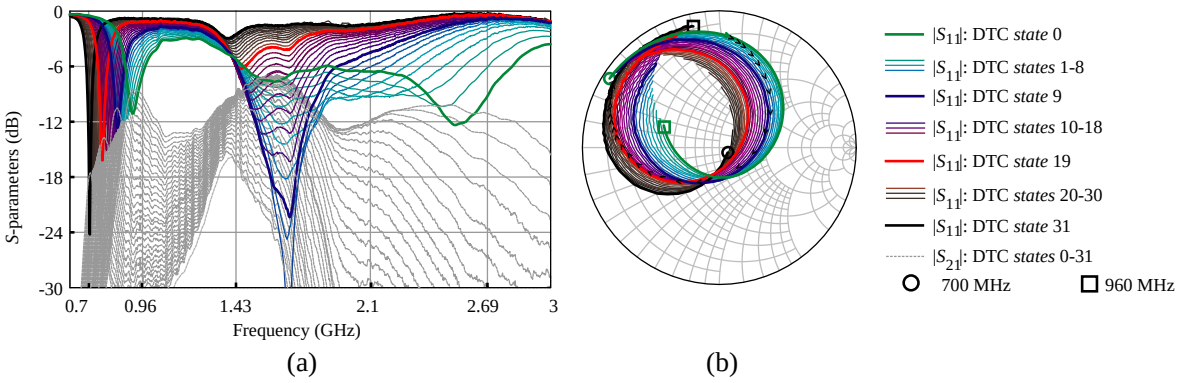

Figure 6. (a) Measured *S*-parameters and (b) input impedances in free space. The DTC states of the elements are changed from 0 to 31. Both elements are operating at the same frequency.

4.2. Free Space

The measured impedance results of *ProtoC* with different DTC states are presented in Figure 6. Both antenna elements are working at the same frequency in order to mimic the worst case scenario. The antenna structure can cover most of the LTE-A bands, and the isolation between the antennas is in the range of 8–18 dB and 7–13 dB at the low- and high-bands, respectively. The antennas can also be tuned to operate at different frequency bands or to compensate the user-originated impedance mistuning. The antenna is matched to have an over-coupled impedance behavior (see Figure 6(b)). This makes the antenna more robust to impedance mistuning caused by user proximity.

Figure 7 presents the measured total efficiency (η_{tot}) results for *ProtoC*. The measured η_{tot} is between −7.0 and −3.0 dB (20–50%) at the low-band, and between −4.0 and −1.0 dB (40–80%) at the high-band. It can be seen that the antenna is fairly selective at the low-band, whereas the selectivity is low the at the high-band. Elements 1 and 2 have similar performance, even though element 1 seems to perform slightly better especially at the low-band due to its position with respect to the enclosure (see Figure 5(c)). The comparison between the simulated and measured efficiencies is shown in Table 1, and a very good agreement is obtained. The performance of the MEMS-based DTC [15] was studied with simulations only. The simulated η_{tot} (*ProtoM*) is between −3.1 and −1.8 dB (49–88%) at the low-band, and between −2.5 and −0.6 dB (56–88%) at the high-band.

4.3. User Effect

In order to verify the robustness of the antenna performance with the user's hand, the antenna prototype was measured with SHO V2RD (later "data grip") hand phantoms by SPEAG. The antenna elements

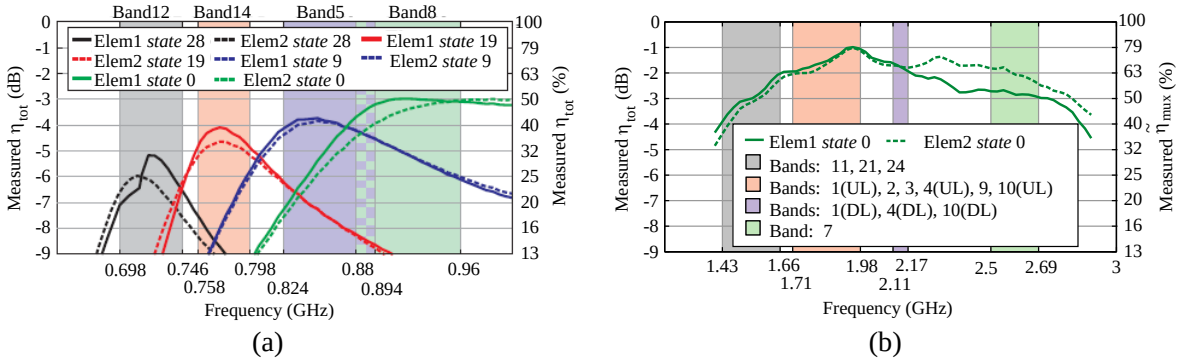

Figure 7. Measured total efficiencies in free space (a) at the low-band, and (b) at the high-band. Elem1 and Elem2 refers to antenna elements 1 and 2, respectively.

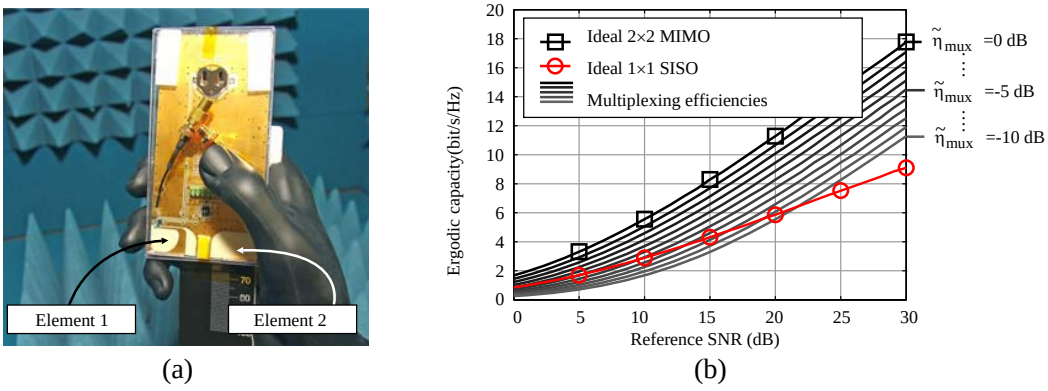

Figure 8. (a) Measurement set-up of *ProtoC* including the data grip. The antenna is located at the 60 mm mark on the hand phantom spacer. (b) Ergodic capacities of different $\tilde{\eta}_{mux}$ values.

are placed at the bottom part of the device in order to fulfill the SAR requirements when the handset is used in a talking position [22–23], as shown in Figure 8(a). The phantom hand is based on the CTIA OTA test plan, revision 3.0.

The measured S-parameters shown in Figure 9(a) suggest that frequency tuning can be used to compensate the user-originated losses. The used DTC states are different compared to the free space case due to the impedance detuning caused by the hand. It can be seen that the tuning range is sufficient, except with element 2 at Band 8, where the matching is not optimal. This is due to a large impedance detuning caused by the palm. With the broader tunability range of the MEMS DTC, more severe user-originated losses can be compensated compared to the CMOS DTC.

In measurements, the total loss was measured and the hand loss was obtained from $\eta_{\text{hand}} = \eta_{\text{tot}}/\eta_{\text{m}}$ where η_{m} is the measured matching loss. The simulated and measured hand losses (see Figure 9(b)) indicate a fairly good agreement. However, in some cases (e.g., Elem 2 at 0.9 GHz), there is approximately a 1.2-dB difference between the measured and simulated η_{hand}. This is mainly due to the insufficient frequency tuning in that particular case, which results in increased uncertainty when estimating η_{hand}. In addition, there is a small uncertainty caused by slight positioning differences between the measured and simulated cases.

The measured hand losses are in the range of 2.6–5.5 dB. At low-band, the hand loss is less dependent on the individual element because the chassis is the main radiator. At high-band, the elements become significant radiators, and therefore a larger part of the losses are concentrated in parts of the hand close to each element. In our measurement setup, element 2 is more affected by the vicinity of the palm tissue than element 1 (see Figure 8(a)). At the low-band, the case is not that straightforward

since the contribution of the chassis at the low-band is more significant than at the high-band: at 0.7 and 0.8 GHz, element 1 causes the largest hand losses, and at 0.9 GHz, the order is reversed.

4.4. MIMO Performance

The measured envelope correlation (ρ_e) and the multiplexing efficiency ($\tilde{\eta}_{mux}$) results in free space and with the user's hand are presented in Figure 10. The measurements were made for *ProtoC*. Because the $\tilde{\eta}_{mux}$ is directly proportional to the efficiency (see Eq. (1)), the improvement in the DTC losses can be directly seen from $\tilde{\eta}_{mux}$. Thus, $\tilde{\eta}_{mux}$ of *ProtoM* will be 0.8–2.8 dB better at the low-band compared to *ProtoC*. At the high-band, the $\tilde{\eta}_{mux}$ performance of the MEMS- and CMOS-based DTCs is roughly the same.

The ρ_e results shown in Figure 10(a) suggest that the user's hand will improve the already good performance at the low-band. At the high-band, the user's hand will improve the ρ_e between 1.43–1.8 GHz, whereas the performance is better without the user at frequencies above 1.8 GHz. The good ρ_e results suggest that the proposed antenna also has a good $\tilde{\eta}_{mux}$ performance (see Figure 10(b)). It can be seen that the user's hand will decrease the $\tilde{\eta}_{mux}$ performance by 3–5 dB at the low-band and by 2–5 dB at the high-band. This agrees with the hand losses discussed in the previous subsection.

The MIMO capacity of the proposed antennas can be estimated from the ergodic capacity presented in Figure 8(b) [24]. The ergodic capacity is calculated by using a Rayleigh fast fading channel. The $\tilde{\eta}_{mux}$ results shown in Figure 10(b) suggest that the channel capacity in free space is decreased by 18–40% and by 7–27% at the low- and high-bands, respectively, compared to the ideal 2x2 MIMO system (SNR = 20 dB). In addition, the ergodic capacity of the proposed antenna outperforms the ideal SISO system even in the worst case when the user's hand is present.

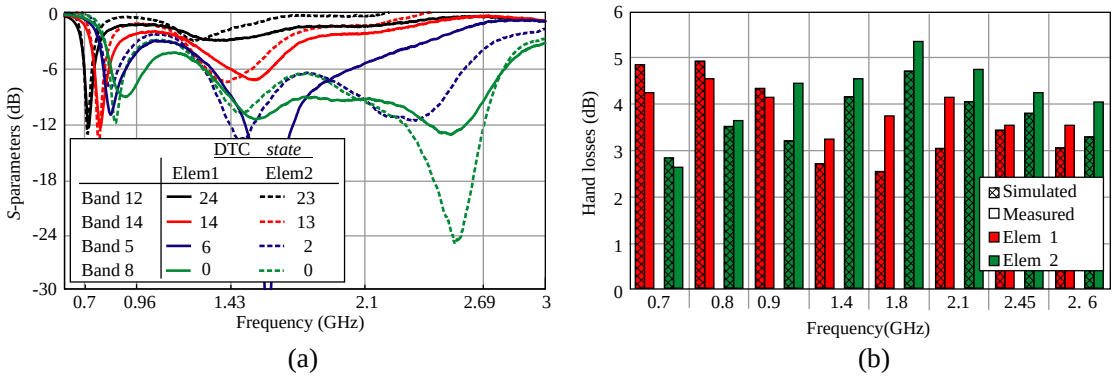

Figure 9. (a) Measured *S*-parameters of *ProtoC* with hand phantom. (b) Simulated and measured hand losses of *ProtoC*.

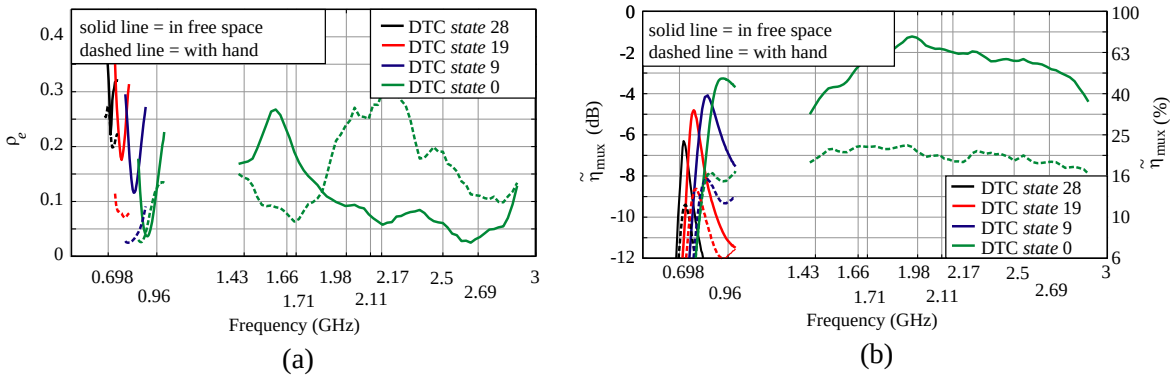

Figure 10. Measured (a) ρ_e and (b) $\tilde{\eta}_{mux}$ of *ProtoC* in free space and with the user's hand.

Table 2. Comparison of LTE MIMO antenna designs presented in this paper and in recent publications. Antenna volume includes the volume of both antennas.

Antenna	Antenna volume (mm^3)	Total dimensions (mm^3)	η_{tot} of main antenna		BW of main antenna		η_{tot} of aux antenna		BW of aux antenna	
			low-band (%)	high-band (%)	low-band (%)	high-band (%)	low-band (%)	high-band (%)	low-band (%)	high-band (%)
Planar ProtoC△	**1170**	**120×60×1.5**	**13–43**	**32–60**	**0.70–0.96**	**1.43–2.69**	**12–43**	**30–60**	**0.70–0.96**	**1.43–2.69**
Planar ProtoM♣	**1170**	**120×60×1.5**	**30–57**	**44–78**	**0.70–0.96**	**1.71–3.60**	**29–57**	**43–78**	**0.70–0.96**	**1.71–3.60**
[1]	2850	115×60×3.8	48–60	63–82	0.70–0.96	1.71–2.69	42–48	50–70	0.70–0.79	2.3–2.69
[2]	3280	100×40×7.8	3–15	6–56	0.74–0.80	2.40–2.80	3–15	6–56	0.74–0.80	2.40–2.80
ProtoC△	**3900**	**120×60×5**	**20–50**	**40–80**	**0.70–0.96**	**1.43–2.69**	**18–50**	**38–79**	**0.70–0.96**	**1.43–2.69**
ProtoM♣	**3900**	**120×60×5**	**49–72**	**56–88**	**0.70–0.96**	**1.43–2.69**	**48–72**	**55–88**	**0.70–0.96**	**1.43–2.69**
[3]	5040	125×60×7	44–54	63–89	0.75–0.96	1.71–2.69	40–43	51–83	0.75–0.96	1.71–2.69
[4]	8640	110×45×6	20–70	40–93	0.73–0.96	1.71–2.50	N/A	N/A	0.75–0.96	1.75–2.55
[5]	8750	100×50×7	35–71	47–87	0.71–0.96	1.73–2.69	48–65	45–72	0.71–0.75	1.73–2.69

△ Measured with CMOS-based DTC. ♣ Simulated with MEMS-based DTC.

4.5. Planar Alternative

Frequency tuning is used to minimize the antenna volume, and thus an extreme case where the antenna height equals the thickness of the substrate ($h = 1.5$ mm) was studied with simulations and measurements. The geometry of the planar structure (later "*Planar Proto*") is the same as the previously presented *Proto*, except that the height of the antenna element is reduced from 5 to 1.5 mm (see Figure 5(a)). The impedance behavior of *Planar Proto* is similar to *Proto* presented in Figure 6. The volume reduction decreases slightly the antenna conductance, i.e., the CLF is increased, and thus the matching circuit losses are increased. If the thinner structure (*Planar ProtoM*) is used instead of the thicker one (*ProtoM*), the η_{tot} is decreased by 0.6–2.1 dB and 0.5–1.1 dB at the low- and high-bands, respectively. The reduction of the η_{tot} with the CMOS-based DTC is about the same order of magnitude as with the MEMS-based DTC. As a conclusion, the antenna volume can be decreased significantly (by ca. 70%) if an extra loss of 0.5–2.1 dB is acceptable.

4.6. Comparison to the State-of-the-Art

In order to identify how the performance of the proposed antenna places it within the state-of-the-art, the proposed antenna is compared to designs presented in recent publications. For fair comparison with the current antenna, the chosen MIMO antennas have fairly similar total dimensions, and they fulfill the LTE-A specification in terms of single antenna bandwidth performance (BW). The emphasis was with the measured η_{tot} results, even though the antenna structures with the MEMS-based DTC are only simulated in this work because of limited availability of the components at the time of the measurements. The η_{tot} results shown in Table 2 are measured in free space. In most of the other structures, the performance of the auxiliary (aux) antenna is limited, while the proposed antenna has almost identical performance of the main and auxiliary antennas. The comparison proves that the antennas presented in this paper (*Planar Proto* and *Proto*) have a very good performance in terms of antenna volume, bandwidth and efficiency.

5. CONCLUSIONS

A novel frequency reconfigurable MIMO handset antenna has been introduced. It is shown that the CLF can be used to estimate the suitability of the antenna geometry for frequency tunable antennas. This paper improves the general understanding of how to design compact and frequency tunable MIMO antennas for mobile handsets while maintaining a good and robust performance with the user. Simulations verify that the antenna has an efficiency better than −3.1 dB (49%) across the frequencies of 698–960 MHz and better than −2.5 dB (56%) across the frequencies of 1430–2690 MHz when a MEMS-based DTC is used. Using a CMOS-based DTC can increase the losses by up to 3 dB. Measurements verify that the antenna has a good spatial multiplexing performance.

ACKNOWLEDGMENT

This work was conducted within the "TAFECO" research project funded by TEKES (Finnish Funding Agency for Technology and Innovation), Nokia Research Center (Espoo, Finland) and Sasken Finland (Kaustinen, Finland), and was also supported by Optenni (Espoo, Finland) and AWR-APLAC (Espoo, Finland). The work of J. Ilvonen was supported in part by the Nokia Foundation and in part by the Finnish Society of Electronics Engineers.

REFERENCES

1. Wong, K.-L., T.-W. Kang, and M.-F. Tu, "Internal mobile phone antenna array for LTE/WWAN and LTE MIMO operations," *Microwave and Optical Technology Letters*, Vol. 53, No. 7, 1569–1573, 2011.
2. Dioum, I., A. Diallfo, S. Farssi, and C. Luxey, "A novel compact dual-band LTE antenna-system for MIMO operation," *IEEE Trans. Antennas Propag.*, Vol. 62, No. 4, 2291–2296, Apr. 2014.
3. Zhang, S., K. Zhao, Z. Ying, and S. He, "Adaptive quad-element multi-wideband antenna array for user-effective LTE MIMO mobile terminals," *IEEE Trans. Antennas Propag.*, Vol. 61, No. 8, 4275–4283, Aug. 2013.
4. Ren, Y.-J., "Ceramic based small LTE MIMO handset antenna," *IEEE Trans. Antennas Propag.*, Vol. 61, No. 2, 934–938, Feb. 2013.
5. Kuonanoja, R., "Low correlation handset antenna configuration for LTE MIMO applications," *IEEE Int. Symp. Antennas and Propagation (APSURSI)*, 1–4, 2010.
6. Ilvonen, J., R. Valkonen, J. Holopainen, and V. Viikari, "Design strategy for 4G handset antennas and a multiband hybrid antenna," *IEEE Trans. Antennas Propag.*, Vol. 62, No. 4, 1918–1927, Apr. 2014.
7. Manteuel, D. and M. Arnold, "Considerations for reconfigurable multi-standard antennas for mobile terminals," *Proc. Int. Workshop Antenna Technology (iWAT)*, 231–234, 2008.
8. Valkonen, R., M. Kaltiokallio, and C. Icheln, "Capacitive coupling element antennas for multi-standard mobile handsets," *IEEE Trans. Antennas Propag.*, Vol. 61, No. 5, 2783–2791, May 2013.
9. Caporal Del Barrio, S., A. Tatomirescu, G. Pedersen, and A. Morris, "Novel architecture for LTE world-phones," *IEEE Antennas Wireless Propag. Lett.*, Vol. 12, 1676–1679, 2013.
10. Payandehjoo, K. and R. Abhari, "Compact multi-band PIFAs on a semi-populated mobile handset with tunable isolation," *IEEE Trans. Antennas Propag.*, Vol. 61, No. 9, 4814–4819, Sep. 2013.
11. Ogawa, K., T. Matsuyoshi, and K. Monma, "An analysis of the performance of a handset diversity antenna influenced by head, hand, and shoulder effects at 900 MHz: Part II — Correlation characteristics," *IEEE Trans. Veh. Technol.*, Vol. 50, No. 3, 845–853, May 2001.
12. Tian, R., B. K. Lau, and Z. Ying, "Multiplexing efficiency of MIMO antennas," *IEEE Antennas Wireless Propag. Lett.*, Vol. 10, 183–186, 2011.
13. Villanen, J., J. Ollikainen, O. Kivekäs, and P. Vainikainen, "Coupling element based mobile terminal antenna structures," *IEEE Trans. Antennas Propag.*, Vol. 54, No. 7, 2142–2153, Jul. 2006.

14. Peregrine, Digitally Tunable Capacitors, Peregrine Semiconductor, San Diego, USA, Online Available: http://www.psemi.com/content/products/product.php?product=PE64904/.
15. WiSpry, Tunable digital capacitor arrays," WiSpry inc., Irvine, USA, Online Available: http://www.wispry.com/products-capacitors.php/.
16. Ilvonen, J., O. Kivekäs, J. Holopainen, R. Valkonen, K. Rasilainen, and P. Vainikainen, "Mobile terminal antenna performance with the user's hand: Effect of antenna dimensioning and location," *IEEE Antennas Wireless Propag. Lett.*, Vol. 10, 772–775, 2011.
17. Rahola, J., "Bandwidth potential and electromagnetic isolation: Tools for analysing the impedance behaviour of antenna systems," *Proc. 3rd European Conf. Antennas and Propagation (EuCAP)*, 944–948, 2009.
18. Zhang, S., K. Zhao, Z. Ying, and S. He, "Diagonal antenna-chassis mode for wideband LTE MIMO antenna arrays in mobile handsets," *Proc. Int. Workshop Antenna Technology (iWAT)*, 407–410, 2013.
19. Optenni Lab, "Matching circuit generation and antenna analysis software," Optenni Ltd., Espoo, Finland, Online Available: http://www.optenni.com/.
20. Lehtovuori, A., R. Valkonen, and J. Ilvonen, "On designing dual-band matching circuits for capacitive coupling element antennas," *Proc. 8th European Conf. Antennas and Propagation, (EuCAP)*, 3909–3913, 2014.
21. Rahola, J., "Effect of antenna Q to the radiation efficiency of tunable antennas," *Proc. 8th European Conf. Antennas and Propagation, (EUCAP)*, 3905–3908, 2014.
22. Zhao, K., S. Zhang, Z. Ying, T. Bolin, and S. He, "SAR study of different MIMO antenna designs for LTE application in smart mobile handsets," *IEEE Trans. Antennas Propag.*, Vol. 61, No. 6, 3270–3279, Jun. 2013.
23. Ilvonen, J., R. Valkonen, O. Kivekäs, P. Li, and P. Vainikainen, "Antenna shielding method reducing the interaction between user and mobile terminal antenna," *Electronics Letters*, Vol. 47, No. 16, 896–897, 2011.
24. Foschini, G. and M. Gans, "On limits of wireless communications in a fading environment when using multiple antennas," *Wireless Pers. Commun.*, Vol. 6, No. 3, 311–335, 1998.